

Magnetic Field Effect on Strained Graphene Junctions

Youness Zahidi^{a,b}, Ilham Redouani^b, Ahmed Jellal^{*b,c} and Hocine Bahlouli^{c,d}

^a*EMAFI, Polydisciplinary Faculty, Sultan Moulay Selimane University, Khouribga, Morocco*

^b*Laboratory of Theoretical Physics, Faculty of Sciences, Chouaïb Doukkali University,
PO Box 20, 24000 El Jadida, Morocco*

^c*Saudi Center for Theoretical Physics, Dhahran, Saudi Arabia*

^d*Physics Department, King Fahd University of Petroleum & Minerals,
Dhahran 31261, Saudi Arabia*

Abstract

We investigate the spin-dependent transport properties of a ferromagnetic/strained/normal graphene junctions with central region subjected to a magnetic field B . An analytical approach, based on Dirac equation, is implemented to obtain the eigenstates and eigenvalues of the charge carrier in three regions. Using the transfer matrix method, we determine the spin-dependent transmission in the presence of an applied strain along the armchair and zigzag directions of the graphene sample. We find that the strain remarkably modifies the Landau levels (LLs) originating from the applied B . It is shown that the spin up/down energy bands, in the first region, are shifted by the exchange H_{ex} and left the whole spectrum linear as in the case of pristine graphene. In the central region, the position of the Dirac point changes due to the uniaxial strain and B . It is also found that the uniaxial strain in graphene induces a contraction of the LLs spectra. Moreover, the strain and B modify the shape and position of some peaks in the transmission probabilities.

PACS numbers: 73.63.-b, 73.23.-b, 72.80.Rj

Keywords: Graphene, strain, spin, magnetic field, Landau levels, transmission.

*a.jellal@ucd.ac.ma

1 Introduction

Graphene remains among the most fascinating and attractive subject in modern physics [1]. This is due to its peculiar physical properties, such as Klein tunneling [2], which describes the tunneling behaviors of relativistic Dirac electrons through a potential barrier. Such an effect has already been observed experimentally [3] in graphene systems. Moreover, the dynamics of the charge carriers obeys a massless Dirac-like equation [4]. The quasi-particles in graphene exhibit a linear dispersion relation in the vicinity of the Dirac point as well as many excellent transport characteristics [1,5]. Furthermore, the development of graphene also opens a new and promising route to nanoelectronics and spintronics because it has a high carrier mobility and small spin-orbit coupling in addition to a long spin coherence length that has reached more than one micrometer at room temperature [6].

It is worth mentioning that the major challenge in designing spintronic devices is the difficulty in generating, controlling and detecting spin polarized currents. The charge carriers in graphene are, in general, not spin polarized. However, the spin polarization is an important concept for novel spintronics application. Recently, it has been suggested [7] that spin polarized carriers can be realized by depositing a ferromagnetic insulator such as EuO on graphene. This can induce an exchange proximity interaction [7,8]. Under the influence of exchange field in ferromagnetic graphene on charge carriers, the current of the system split into spin up and spin down current components. This effect is due to the so-called Zeeman effect, which gives rise to spin polarization. The deposition of ferromagnetic insulator EuO on the graphene sheet was experimentally realized [9]. It has been theoretically predicted that the spin current can be controlled by gate voltages [7,10], magnetic barriers [11,12] and local strain [13,14].

Graphene, a one-atom-thick film, exhibits a truly two-dimensional nature, which is considered as a flexible membrane. Thus, it is possible to connect mechanical properties with the electronic ones. This opens the way to investigate the interplay between elastic and electronic properties [15–17]. The electronic properties of graphene based nanostructures can be tuned by performing a deformation on the graphene sample [7,18–20]. The applied strain in graphene can be controlled using different methods [16]. The application of a strain on graphene sheet acts on the Dirac fermions as a pseudomagnetic field [21]. Experimentally, it has been found that the application of strain on graphene nanobubble leads to a huge pseudo-magnetic field ($< 300 T$), that has never been created in the laboratory [15]. Thus, a uniaxial strain larger than 23% in the zigzag direction can generate a transport gap in the transmission [22,23]. Importantly, mechanical strains in graphene can also shift the Dirac points, which causes the Dirac fermions to have asymmetrical velocity $v_x \neq v_y$ [17,24].

We plan to investigate the effect of an applied magnetic field on the spin transport properties of a ferromagnetic/strained/normal graphene junctions. The present system is made up of three regions where the central one is subjected to the uniaxial strain and B . After writing down the Hamiltonian for each region, we solve the corresponding Dirac equation to obtain eigenspinors and eigenvalues. Using the boundary conditions together with transfer matrix approach, we determine the transmission probabilities in terms of the physical parameters. The strain effects (along armchair and zigzag directions) on the transmission for zero and non-zero magnetic field will be analyzed. We show that strain reduces the transmission along the zigzag direction and increases the transmission along the armchair direction.

The manuscript is organized as follows. In section 2, we set the theoretical model involving the Hamiltonians describing each region of our system. These will be used to separately solve Dirac equation to obtain the solutions of the energy spectrum and in particular the Landau levels in the central region. In section 3, we explicitly determine the corresponding transmission probabilities in terms of the physical parameters. In section 4, We numerically analyze our results under suitable configurations of the physical parameters characterizing our system. We conclude our work in the final section.

2 Model for a uniaxial strained graphene

We consider a graphene based system, which is made of three regions as shown in Figure 1(a). A ferromagnetic/strained/normal graphene junction, where a uniaxial strained graphene sheet of width ω is sandwiched between a ferromagnetic and normal metal which are deposited, respectively, on the left and right regions. Depositing a ferromagnetic metal, such as EuO, on graphene can induce an exchange proximity interaction, which can be treated as an effective exchange field [7, 8]. In the central region, we apply a magnetic field perpendicular to the graphene layer along the z -direction.

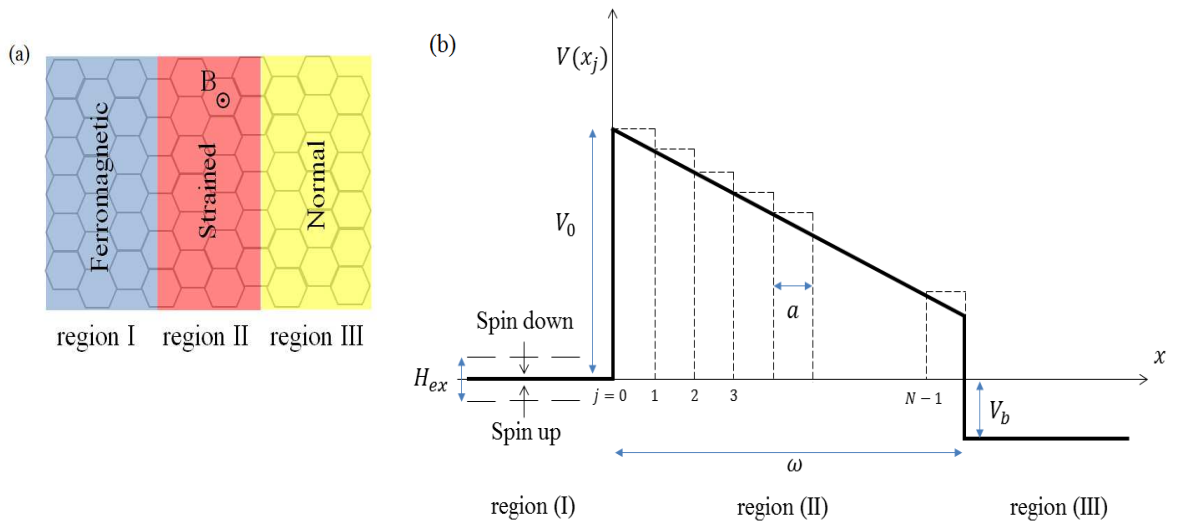


Figure 1: (color online) (a): Schematic illustration of the ferromagnetic/strained/normal graphene junction with a magnetic field in the strained region. (b): Potential diagram in different regions with the exchange field H_{ex} , potential V_0 , bias V_b , width of the strained region ω and step of discrimination a .

The effective Hamiltonian describing the quasi-particles in this graphene-based system in the presence of a magnetic field can be written as

$$\hat{H}_{F,\eta} = v_F(\sigma_x \pi_{x_1} + \sigma_y \pi_{y_1}) - \eta H_{ex} \sigma_0 \quad (1)$$

$$\hat{H}_S = v_F U^\dagger(\theta) [\sigma_x (1 - \lambda_x \varepsilon) \pi_{x_2} + \sigma_y (1 - \lambda_y \varepsilon) \pi_{y_2}] U(\theta) + (V_0 - \beta x) \sigma_0 \quad (2)$$

$$\hat{H}_N = v_F(\sigma_x \pi_{x_3} + \sigma_y \pi_{y_3}) - V_b \sigma_0 \quad (3)$$

where $v_F = 10^6 m/s$ is the Fermi velocity, σ_x and σ_y are Pauli matrices in pseudospin space, σ_0 is the 2×2 unit matrix, $\eta = +/ - 1$ refer to up/down spin orientation, H_{ex} is the exchange field,

$U^+(\theta) = \text{diag}(1, e^{+i\theta})$ is the unitary matrix, θ is the angle between the strain direction and the graphene zigzag direction, ε is the magnitude of the strain, $\lambda_x \approx 2.2$ and $\lambda_y \approx -0.308$. Note that in the presence of a bias V_b and because of the uniform in-plane electric field between the left and right electrodes, a linear voltage drop with a dropping factor of $\beta = \frac{V_b}{\omega}$, as shown in Figure 1(b) [25–27]. In addition, the potential barrier V_0 will lift the linear voltage drop completely because of V_0 is induced by the strain or by an additional gate in the middle region of width ω . In this work, we consider a magnitude of the strain limited within 20%, which means that the energy gap cannot be opened up [16]. The conjugate momenta in the Landau gauge are given by

$$\pi_{x_i} = p_x = \hbar q_x = -i\hbar\partial_x \quad (4)$$

$$\pi_{y_i} = p_y + \frac{e}{c}A_{x_i} = \hbar q_y + \frac{e}{c}A_{x_i} = -i\hbar\partial_y + \frac{e}{c}A_{x_i} \quad (5)$$

and due to the continuity, the vector potential in the three regions takes the form

$$A_{x_i} = \frac{c\hbar}{el_B^2} \begin{cases} 0, & x \leq 0 \\ x, & 0 < x < \omega \\ \omega, & x \geq \omega \end{cases} \quad (6)$$

with $l_B \equiv \sqrt{\frac{c\hbar}{eB}}$ is the magnetic length and $i = \text{I, II, III}$ labels the three regions. Now we can rewrite the Hamiltonian as

$$\hat{H}_{F,\eta} = v_F(\sigma_x p_x + \sigma_y p_y) - \eta H_{ex} \sigma_0 \quad (7)$$

$$\hat{H}_S = v_F U^\dagger(\theta) \left[\sigma_x (1 - \lambda_x \varepsilon) \hbar q_x + \sigma_y (1 - \lambda_y \varepsilon) \left(\hbar q_y + \frac{\hbar x}{l_B^2} \right) \right] U(\theta) + (V_0 - \beta x) \sigma_0 \quad (8)$$

$$\hat{H}_N = v_F \left(\sigma_x p_x + \sigma_y \left(p_y + \frac{\hbar \omega}{l_B^2} \right) \right) - V_b \sigma_0 \quad (9)$$

and the components q_x and q_y , measure the wave vector displacements from the shifted Dirac points [26], such that

$$q_D a_0 = \pm (k_0 \varepsilon (1 + \mu) \cos(3\theta), -k_0 \varepsilon (1 + \mu) \sin(3\theta)) \quad (10)$$

with two quantities $k_0 \approx 1.6$ and $a_0 = 0.142 \text{ nm}$.

By considering the conservation of the transverse wave vector k_y and using (7-9), we can write the eigenspinors of these quasi-particles, moving along the $\pm x$ -directions, in all regions as $\Phi^\pm(x, y) = \psi^\pm(x) e^{ik_y y}$. Thus, the solution in the ferromagnetic region I can be obtained as

$$\psi_I(x) = \begin{pmatrix} 1 \\ g_\eta e^{i\gamma_\eta} \end{pmatrix} e^{ik_\eta x} + r_\eta \begin{pmatrix} 1 \\ -g_\eta e^{-i\gamma_\eta} \end{pmatrix} e^{-ik_\eta x} \quad (11)$$

where $g_\eta = \text{sign}(E + \eta H_{ex})$, the angle and wave vector are given by

$$\gamma_\eta = \sin^{-1} \left(\frac{\hbar v_F k_y}{|E + \eta H_{ex}|} \right), \quad k_\eta = \frac{|E + \eta H_{ex}|}{\hbar v_F} \cos \gamma_\eta \quad (12)$$

giving rise to the eigenvalues

$$E = g_\eta \hbar v_F \sqrt{k_\eta^2 + k_y^2} - \eta H_{ex}. \quad (13)$$

In the third region III we get the solution

$$\psi_{\text{III}}(x) = t_\eta \begin{pmatrix} 1 \\ \chi e^{i\phi} \end{pmatrix} e^{ik_x x} \quad (14)$$

with $\chi = \text{sign}(E + V_b)$, the angle and wave vector read as

$$\phi = \sin^{-1} \left(\frac{\hbar v_F (k_y + \frac{\omega}{l_B^2})}{|E + V_b|} \right), \quad k_x = \frac{|E + V_b|}{\hbar v_F} \cos \phi \quad (15)$$

and the corresponding eigenvalues are

$$E = \chi \hbar v_F \sqrt{k_x^2 + \left(k_y + \frac{\omega}{l_B^2} \right)^2} - V_b. \quad (16)$$

In the strained region II the components of the eigenspinors are no longer plane waves because of the potential drop. To arrive at approximate results, we have split region 2 into series of reasonably uniform widths $a = \omega/N \gg a_0$ (see Figure 1(b)), whose potential is considered almost constant. In such case, these components can be considered approximately as plane waves with $\alpha_j = j \times a$ ($j = 0, 1, 2, \dots, N$) and N is the number of narrow layers. The Hamiltonian of j^{th} narrow layer is given by

$$H_{S,j} = \hbar v_F U^\dagger(\theta) \left[\sigma_x (1 - \lambda_x \varepsilon) q_x + \sigma_y (1 - \lambda_y \varepsilon) \left(q_y + \frac{x}{l_B^2} \right) \right] U(\theta) + (V_0 - \beta \alpha_j) \sigma_0 \quad (17)$$

satisfying the eigenvalue equation

$$H_{S,j} \Phi_{S,j}(x, y) = E \Phi_{S,j}(x, y) \quad (18)$$

which can explicitly be written as

$$-i \hbar v_F (1 - \lambda_x \varepsilon) \left(\partial_x + \frac{1 - \lambda_y \varepsilon}{1 - \lambda_x \varepsilon} \left(k_y - q_{D_y} + \frac{x}{l_B^2} \right) \right) e^{-i\theta} \psi_{\parallel}^B(x) = (E + \beta \alpha_j - V_0) \psi_{\parallel}^A(x) \quad (19)$$

$$i \hbar v_F (1 - \lambda_x \varepsilon) \left(-\partial_x + \frac{1 - \lambda_y \varepsilon}{1 - \lambda_x \varepsilon} \left(k_y - q_{D_y} + \frac{x}{l_B^2} \right) \right) e^{+i\theta} \psi_{\parallel}^A(x) = (E + \beta \alpha_j - V_0) \psi_{\parallel}^B(x). \quad (20)$$

Making use of the variable change $X = l_B \sqrt{\alpha} \left(k_y - q_{D_y} + \frac{x}{l_B^2} \right)$ and strain parameter $\alpha = \frac{1 - \lambda_y \varepsilon}{1 - \lambda_x \varepsilon}$ to map (19-20) as

$$-i \hbar v_F (1 - \lambda_x \varepsilon) \frac{\sqrt{\alpha}}{l_B} (\partial_X + X) e^{-i\theta} \psi_{\parallel}^B(x) = (E + \beta \alpha_j - V_0) \psi_{\parallel}^A(x) \quad (21)$$

$$i \hbar v_F (1 - \lambda_x \varepsilon) \frac{\sqrt{\alpha}}{l_B} (-\partial_X + X) e^{+i\theta} \psi_{\parallel}^A(x) = (E + \beta \alpha_j - V_0) \psi_{\parallel}^B(x) \quad (22)$$

which can be solved by introducing the usual bosonic operators

$$a^\dagger = \frac{1}{\sqrt{2}} (-\partial_X + X), \quad a = \frac{1}{\sqrt{2}} (\partial_X + X) \quad (23)$$

satisfying the commutation relation $[a, a^\dagger] = \mathbb{I}$. Thus, we write

$$-i \hbar v_F \frac{\sqrt{2\alpha}}{l_B} (1 - \lambda_x \varepsilon) a e^{-i\theta} \psi_{\parallel}^B(x) = (E + \beta \alpha_j - V_0) \psi_{\parallel}^A(x) \quad (24)$$

$$i \hbar v_F \frac{\sqrt{2\alpha}}{l_B} (1 - \lambda_x \varepsilon) a^\dagger e^{+i\theta} \psi_{\parallel}^A(x) = (E + \beta \alpha_j - V_0) \psi_{\parallel}^B(x) \quad (25)$$

giving rise to the second order differential equation for $\psi_{\parallel}^A(x)$

$$\frac{2\alpha}{l_B^2}(1 - \lambda_x \varepsilon)^2 a a^\dagger \psi_2^A(x) = \left(\frac{E + \beta\alpha_j - V_0}{\hbar v_F} \right)^2 \psi_{\parallel}^A(x). \quad (26)$$

It is clear that (26) is similar to that describing the harmonic oscillator in one dimension and therefore we can identify ψ_{\parallel}^A to be a harmonic oscillator eigenstate

$$\psi_{\parallel}^A \sim |n-1\rangle \quad (27)$$

associated to the eigenvalues

$$E_{n,j} = \pm \hbar v_F \frac{1 - \lambda_x \varepsilon}{l_B} \sqrt{2\alpha n} + V_0 - \beta\alpha_j \quad (28)$$

and the second spinor component can be obtained by injecting (27) into (25)

$$\psi_{\parallel}^B = i \frac{\sqrt{2\alpha} e^{+i\theta}}{l_B \left(\frac{E + \beta\alpha_j - V_0}{\hbar v_F} \right)} (1 - \lambda_x \varepsilon) a^\dagger |n-1\rangle. \quad (29)$$

It is convenient to work with the parabolic cylindrical functions

$$D_n(x) = 2^{-\frac{n}{2}} e^{-\frac{x^2}{4}} H_n \left(\frac{x}{\sqrt{2}} \right) \quad (30)$$

and express the solution in the central region as

$$\psi_{\parallel}(x_j) = a_j \psi_{\parallel}^+(x_j) + b_j \psi_{\parallel}^-(x_j) \quad (31)$$

where the components are given by

$$\psi_{\parallel}^{\pm}(x_j) = \begin{pmatrix} D_{n-1} \left[\pm \sqrt{2\alpha} \left(l_B(k_y - q_{D_y}) + \frac{x_j}{l_B} \right) \right] \\ \pm i \Omega_j e^{+i\theta} D_n \left[\pm \sqrt{2\alpha} \left(l_B(k_y - q_{D_y}) + \frac{x_j}{l_B} \right) \right] \end{pmatrix} \quad (32)$$

with (a_j, b_j) are two constants and we have set the quantity

$$\Omega_j = \frac{\hbar v_F \sqrt{2\alpha} (1 - \lambda_x \varepsilon)}{l_B |E_{n,j} + \beta\alpha_j - V_0|}. \quad (33)$$

It is clearly seen that the above solutions show strong dependency on the strain and magnetic field effects. In the forthcoming analysis, we will study their influence on the transmission of the charge carriers through the considered potential barrier.

3 Transmission probabilities

We analyze the strain effect on the transmission probability in ferromagnetic/strained/normal graphene junction under magnetic field. To determine the transmission and reflection probabilities, we use the corresponding current densities

$$T_\eta = \left| \frac{j_{\text{tra}}^\eta}{j_{\text{inc}}^\eta} \right|, \quad R_\eta = \left| \frac{j_{\text{ref}}^\eta}{j_{\text{inc}}^\eta} \right| \quad (34)$$

where $(j_{\text{inc}}^\eta, j_{\text{ref}}^\eta, j_{\text{tra}}^\eta)$ are, respectively, the probability current density of the incident, reflected and transmitted waves. For a relativistic quasi-particle propagating along the positive x -direction, the current density is given by

$$J = ev_F \bar{\psi} \sigma_x \psi \quad (35)$$

and therefore we derive the results

$$j_{\text{inc}}^\eta = 2ev_F \frac{k_\eta}{E + \eta H_{ex}} \quad (36)$$

$$j_{\text{ref}}^\eta = -2ev_F \frac{k_\eta}{E + \eta H_{ex}} r_\eta^* r_\eta \quad (37)$$

$$j_{\text{tra}}^\eta = 2ev_F \frac{k_x}{E + V_b} t_\eta^* t_\eta \quad (38)$$

leading to the probabilities

$$T_\eta = \left| \frac{j_{\text{tra}}^\eta}{j_{\text{inc}}^\eta} \right| = \frac{k_x (E + \eta H_{ex})}{k_\eta (E + V_b)} |t_\eta|^2 \quad (39)$$

$$R_\eta = \left| \frac{j_{\text{ref}}^\eta}{j_{\text{inc}}^\eta} \right| = |r_\eta|^2. \quad (40)$$

To go further, we need to determine the transmission t_η and reflection r_η coefficients. Indeed, since the quasi-particles have normalized probability densities, then we can write the eigenspinors corresponding to the three regions as

$$\Phi(x, y) = \begin{cases} U^+(\theta) \psi_{\text{I}}(x) e^{ik_y y}, & x \leq 0 \\ U^+(\theta) \psi_{\text{II}}(x) e^{ik_y y}, & 0 < x < \omega \\ U^+(\theta) \psi_{\text{III}}(x) e^{ik_y y}, & x \geq \omega \end{cases} \quad (41)$$

where different eigenspinors in x -direction take the forms

$$\psi_{\text{I}}(x) = \begin{pmatrix} 1 \\ g_\eta e^{i\gamma_\eta} \end{pmatrix} e^{+ik_\eta x} + r_\eta \begin{pmatrix} 1 \\ -g_\eta e^{-i\gamma_\eta} \end{pmatrix} e^{-ik_\eta x} \quad (42)$$

$$\begin{aligned} \psi_{\text{II}}(x_j) &= a_j \begin{pmatrix} D_{n-1} \left[+\sqrt{2\alpha} \left(l_B(k_y - q_{D_y}) + \frac{x_j}{l_B} \right) \right] \\ +i\Omega_j e^{+i\theta} D_n \left[+\sqrt{2\alpha} \left(l_B(k_y - q_{D_y}) + \frac{x_j}{l_B} \right) \right] \end{pmatrix} \\ &+ b_j \begin{pmatrix} D_{n-1} \left[-\sqrt{2\alpha} \left(l_B(k_y - q_{D_y}) + \frac{x_j}{l_B} \right) \right] \\ -i\Omega_j e^{+i\theta} D_n \left[-\sqrt{2\alpha} \left(l_B(k_y - q_{D_y}) + \frac{x_j}{l_B} \right) \right] \end{pmatrix} \end{aligned} \quad (43)$$

$$\psi_{\text{III}}(x) = t_\eta \begin{pmatrix} 1 \\ \chi e^{+i\phi} \end{pmatrix} e^{+ik_x x} \quad (44)$$

with $j = 0, 1, 2, \dots, N$ and N is the number of narrow layers. To determine the coefficients r_η , t_η , a_j and b_j using the continuity equations, we define the shorthand notations

$$\eta_j^\pm(x_j) = D_{n-1} \left[\pm\sqrt{2\alpha} \left(l_B(k_y - q_{D_y}) + \frac{x_j}{l_B} \right) \right] \quad (45)$$

$$\delta_j^\pm(x_j) = \pm i\Omega_j D_n \left[\pm\sqrt{2\alpha} \left(l_B(k_y - q_{D_y}) + \frac{x_j}{l_B} \right) \right]. \quad (46)$$

The continuity of the eigenspinors (41) at each interface results in a set of equations. Indeed, at the x_j ($j = 0, 1, 2, \dots, N$), we have, respectively, for $x = 0$, $x = a$, $x = 2a \dots$ and $x = Na = \omega$

$$\begin{cases} 1 + r_\eta = \eta_0^+ a_0 + \eta_0^- b_0 \\ g_\eta e^{i\gamma_\eta} - g_\eta r_\eta e^{-i\gamma_\eta} = i\delta_0^+ a_0 - i\delta_0^- b_0 \end{cases} \quad (47)$$

$$\begin{cases} \eta_0^+(a) a_0 + \eta_0^-(a) b_0 = \eta_1^+(a) a_1 + \eta_1^-(a) b_1 \\ i\delta_0^+(a) a_0 - i\delta_0^-(a) b_0 = i\delta_1^+(a) a_1 - i\delta_1^-(a) b_1 \end{cases} \quad (48)$$

$$\begin{cases} \eta_1^+(2a) a_1 + \eta_1^-(2a) b_1 = \eta_2^+(2a) a_2 + \eta_2^-(2a) b_2 \\ i\delta_1^+(2a) a_1 - i\delta_1^-(2a) b_1 = i\delta_2^+(2a) a_2 - i\delta_2^-(2a) b_2 \end{cases} \quad (49)$$

⋮

$$\begin{cases} \eta_{N-1}^+(Na) a_{N-1} + \eta_{N-1}^-(Na) b_{N-1} = t_\eta e^{ik_x w} \\ i\delta_{N-1}^+(Na) a_{N-1} - i\delta_{N-1}^-(Na) b_{N-1} = \chi e^{i\varphi} t_\eta e^{ik_x w} \end{cases} \quad (50)$$

which can be cast as

$$\begin{pmatrix} 1 \\ r_\eta \end{pmatrix} = \begin{pmatrix} 1 & 1 \\ g_\eta e^{i\gamma_\eta} & -g_\eta e^{-i\gamma_\eta} \end{pmatrix}^{-1} \begin{pmatrix} \eta_0^+(0) & \eta_0^-(0) \\ i\delta_0^+(0) & -i\delta_0^-(0) \end{pmatrix} \begin{pmatrix} \eta_0^+(a) & \eta_0^-(a) \\ i\delta_0^+(a) & -i\delta_0^-(a) \end{pmatrix}^{-1} \\ \begin{pmatrix} \eta_1^+(a) & \eta_1^-(a) \\ i\delta_1^+(a) & -i\delta_1^-(a) \end{pmatrix} \begin{pmatrix} \eta_1^+(2a) & \eta_1^-(2a) \\ i\delta_1^+(2a) & -i\delta_1^-(2a) \end{pmatrix}^{-1} \begin{pmatrix} \eta_2^+(2a) & \eta_2^-(2a) \\ i\delta_2^+(2a) & -i\delta_2^-(2a) \end{pmatrix} \\ \begin{pmatrix} \eta_2^+(3a) & \eta_2^-(3a) \\ i\delta_2^+(3a) & -i\delta_2^-(3a) \end{pmatrix}^{-1} \dots \begin{pmatrix} \eta_{N-1}^+(Na) & \eta_{N-1}^-(Na) \\ i\delta_{N-1}^+(Na) & -i\delta_{N-1}^-(Na) \end{pmatrix}^{-1} \\ \begin{pmatrix} e^{ik_x w} & e^{-ik_x w} \\ \chi e^{ik_x w} e^{i\phi} & -\chi e^{-ik_x w} e^{-i\phi} \end{pmatrix} \begin{pmatrix} t_\eta \\ 0 \end{pmatrix} \quad (51)$$

or equivalently to

$$\begin{pmatrix} 1 \\ r_\eta \end{pmatrix} = \begin{pmatrix} 1 & 1 \\ g_\eta e^{i\gamma_\eta} & -g_\eta e^{-i\gamma_\eta} \end{pmatrix}^{-1} \prod_{j=0}^{N-1} \tau_j \sigma_j^{-1} \begin{pmatrix} e^{ik_x w} & e^{-ik_x w} \\ \chi e^{ik_x w} e^{i\phi} & -\chi e^{-ik_x w} e^{-i\phi} \end{pmatrix} \begin{pmatrix} t_\eta \\ 0 \end{pmatrix} \quad (52)$$

where we have set the quantities

$$\tau_j = \begin{pmatrix} \eta_j^+(ja) & \eta_j^-(ja) \\ \delta_j^+(ja) & \delta_j^-(ja) \end{pmatrix}, \quad \sigma_j = \begin{pmatrix} \eta_j^+((j+1)a) & \eta_j^-((j+1)a) \\ \delta_j^+((j+1)a) & \delta_j^-((j+1)a) \end{pmatrix} \quad (53)$$

We show that (52) can be written in compact form as

$$\begin{pmatrix} 1 \\ r_\eta \end{pmatrix} = \begin{pmatrix} M_{11}^\eta & M_{12}^\eta \\ M_{21}^\eta & M_{22}^\eta \end{pmatrix} \begin{pmatrix} t_\eta \\ 0 \end{pmatrix} \quad (54)$$

and the coefficients are given by

$$t_\eta = \frac{1}{M_{11}^\eta}, \quad r_\eta = \frac{M_{21}^\eta}{M_{11}^\eta} \quad (55)$$

leading to the transmission and reflection probabilities

$$T_\eta = \frac{k_x (E + \eta H_{ex})}{k_\eta (E + V_b)} \frac{1}{(M_{11}^\eta)^* M_{11}^\eta}, \quad R_\eta = \left(\frac{M_{21}^\eta}{M_{11}^\eta} \right)^* \frac{M_{21}^\eta}{M_{11}^\eta}. \quad (56)$$

The obtained results so far will be analyzed numerically and discussed using some suitable selections of the physical parameters characterizing our system.

4 Results and discussions

We will investigate the physical behavior of our system using a numerical implementation of the previous theoretical model to compute the energy spectrum, transmission probability and examine the magnetic field and strain effects. First, we define nanostructures derived from graphene, called nanorribbons of graphene. These are unidimensional graphene-based structures as shown in Figure 1, which possess remarkable properties especially under the effects of the electric and magnetic fields. For this, we consider two typical strain directions including the zigzag ($\theta = 0$) and armchair ($\theta = \frac{\pi}{2}$) directions.

Before proceeding to discuss spin-dependent transmission, we will study the respective energy spectrum in each region of the considered device. In the left region (I) the dispersion relation is described by (13) and the energy bands are illustrated in Figure 2(a). We clearly see that the spin up and down bands are shifted by an amount equal to the exchange energy H_{ex} and left the whole spectrum linear as in the case of pristine graphene. The dispersion relation, in the right region (III) is described by (16) and in Figure 2(b) we show the energy spectrum for different values of the magnetic field B . We observe that for zero magnetic field, the energy bands are linear and similar to those in pristine graphene, but shifted down by V_b due to the bias. By increasing B , we see that the energy spectrum is still linear, but the Dirac point is shifted and such shift is as a consequence of the uniaxial strain applied in the central region (II) as already found in [26].

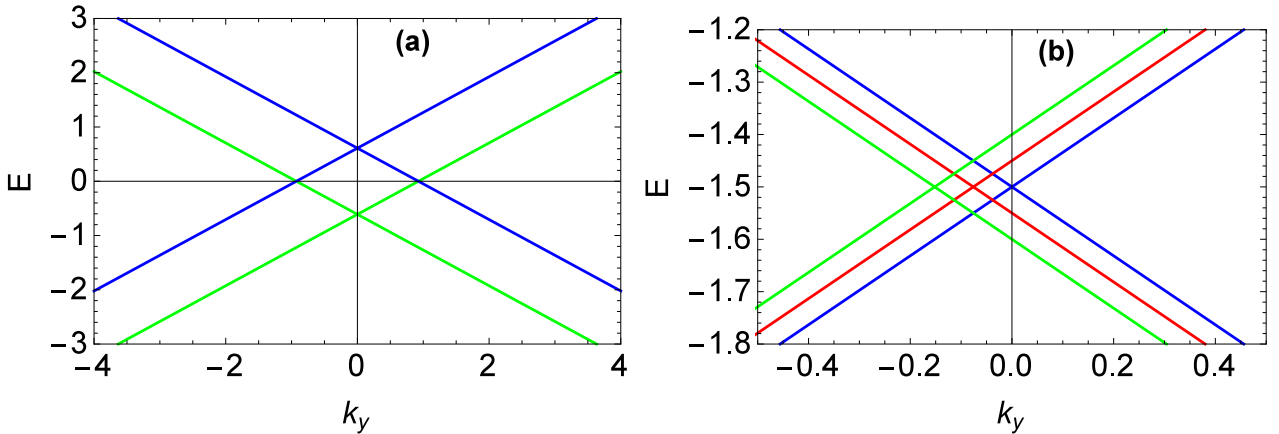


Figure 2: (color online) (a): Energy bands of region I as a function of the momentum k_y with $H_{ex} = 0.61 \text{ meV}$, green and blue lines correspond, respectively, to upper ($\eta = +1$) and lower ($\eta = -1$) spin. (b): Energy bands of region III as a function of the momentum k_y with $V_b = 1.5 \text{ meV}$, $\omega = 1 \text{ nm}$, blue, red and green lines correspond to $B = 0 \text{ T}$, $B = 50 \text{ T}$ and $B = 100 \text{ T}$, respectively

In the central region (II), the story is completely different because besides the strain effect we have also a perpendicular magnetic field that leaves the energy spectrum quantized, which results in the so-called Landau levels (LLs), see (28). The evolution of the LLs spectra as a function of the strain ε is shown in Figure 4(a). To thoroughly examine the effect of strain on LLs, we rewrite (28) as

$$E_{n,j} = \pm \hbar \omega_c \xi \sqrt{n} + V_0 - \beta \alpha_j, \quad n \in \mathbb{N}, \quad j = 0, 1, 2, \dots, N \quad (57)$$

where $\omega_c = v_F \frac{\sqrt{2}}{\gamma_B}$ is the cyclotron frequency and $\xi = \sqrt{(1 - \lambda_x \varepsilon)(1 - \lambda_y \varepsilon)}$ is a parameter of strain.

Moreover, one sees that the first term in (57) is similar to that corresponding to pristine graphene in magnetic field B apart from a renormalization of the Fermi velocity $v_F^* = \xi v_F$ [28]. Furthermore, ξ is considered as a parameter to measure the contraction or the expansion ($\xi < 1$ or $\xi > 1$) of the LLs spectra under the same magnetic field. It should be noticed that the limiting case $\xi = 1$ corresponds actually to pristine graphene.

In Figure 3, we show the evolution of the ξ parameter as a function of the strain ε . It is clearly shown that, $\xi = 1$ for $\varepsilon = 0$ ($v_F^* = v_F$), which corresponds to pristine graphene and confirm what we have already mentioned above. By increasing the strain ε , the parameter ξ decreases [28] and automatically v_F^* decreases. From this Figure, it is clearly seen that whatever the strain deformation (under 20 %) we have $\xi < 1$, which means that the LLs are contracted compared to the pristine graphene.

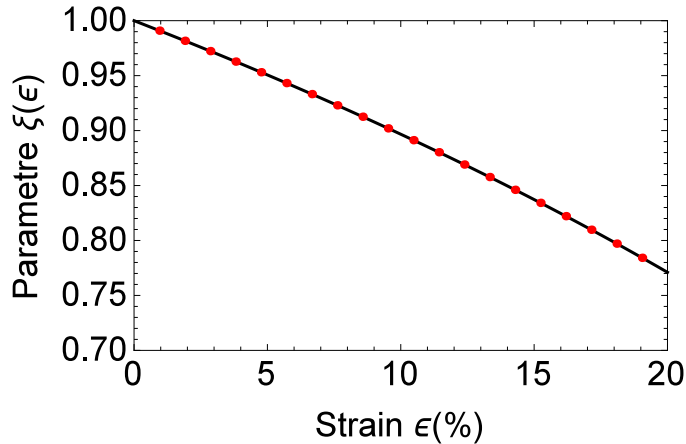


Figure 3: (color online) Evolution of the parameter ξ for strained graphene as a function of the strain ε .

From Figure 4(a), we clearly see that under the same magnetic field, the energy decreases by increasing the magnitude ε of the uniaxial strain. Moreover, the distance between the LLs decreases as well by increasing ε . Thus, the LLs spectra are contracted, which means that $\xi < 1$, as compared to pristine graphene ($\xi = 1$). This can be explained by the fact that the induced uniaxial strain affects the cyclotron orbital motion. It is important to mention that this result is similar to that obtained in [29]. To show the effect of the applied magnetic field, we plot the energy as a function of the magnetic field in Figure 4(b). Note that the LLs spectra (28) depend on the square root of both the level index n and the magnetic field B . From this Figure, we can show that for zero magnetic field the energy is not degenerate and by increasing B the LLs increase and become degenerate.

As we mentioned earlier, the strain can be applied along either the ZZ or AC directions. In Figure 5 we show the spin-dependent transmission probability as a function of the energy for different strengths of the strain along the ZZ and AC directions, respectively. We notice that when the deformation is increased along the ZZ direction ($\theta = 0$) or AC direction ($\theta = \frac{\pi}{2}$), it is found that the zone in which the transmission is minimal can reach zero at a certain values of the energy (*i.e.* transmission gap) corresponding to the forbidden band. Moreover, introducing a ZZ strain leaves the transmission profile almost unchanged such that the associated peaks are located at fixed energy. However, the overall transmission probability is significantly reduced, see Figure 5(a). In addition, when the strain follows the ZZ direction, the forbidden zone becomes larger by increasing the strength of the strain. In

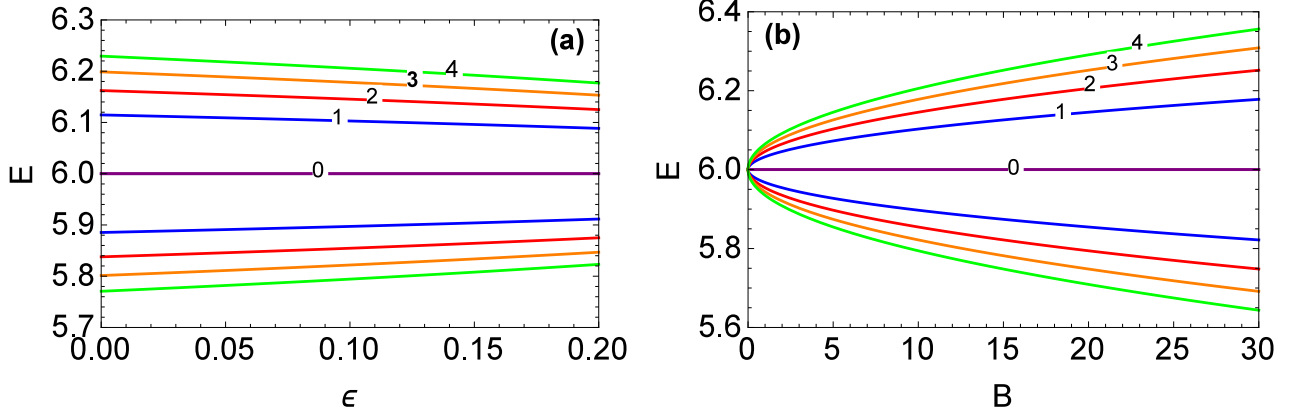


Figure 4: (color online) (a): Energy bands of region II as a function of the strain ε with $B = 10 T$, $\omega = 0.1 nm$ and $n = 0, \dots, 4$. (b): Energy bands of region II as a function of the magnetic field B with $\omega = 0.2 nm$, $\varepsilon = 0.1$, $V_b = 6$ and $n = 0, \dots, 4$.

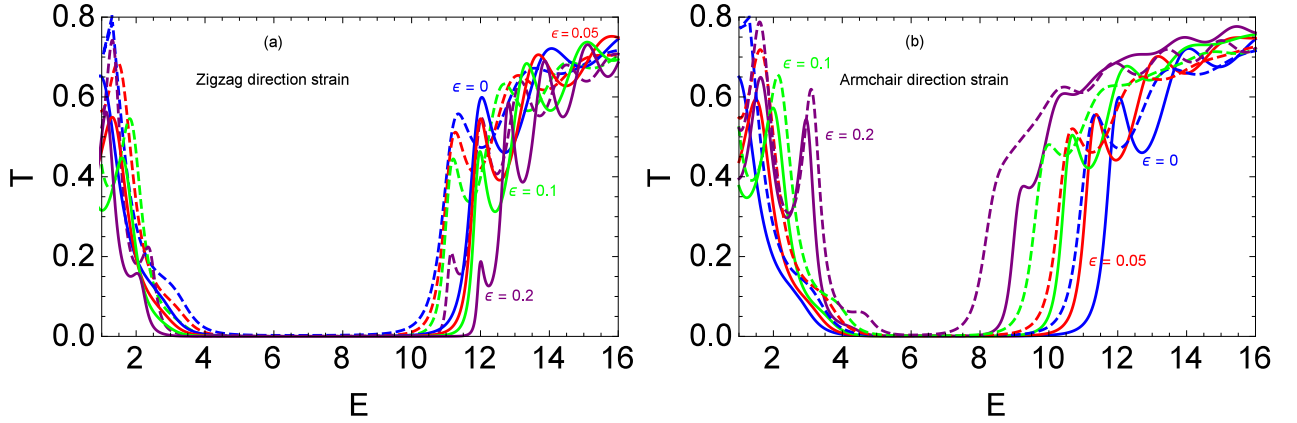


Figure 5: (color online) Transmission probability as a function of the energy for different strains $\varepsilon = 0.00, 0.05, 0.10$, and 0.20 . (a): Effects of zigzag strain direction for up/down spin $\eta = +/- 1$. (b): The effects of armchair strain direction for up/down spin $\eta = +/- 1$ ($\eta = 1$: solid line, $\eta = -1$: dashed line). Other parameters are $\gamma_\eta = 38^\circ$, $\omega = 0.8 nm$, $H_{ex} = 0.61 meV$, $V_b = 1.5 meV$, $V_0 = 6 meV$, $l_B = 0.5 nm$.

contrast, when we introduce a ZZ strain the transmission gap (*i.e.* $T = 0$) becomes wider by decreasing the strength of the strain as shown in Figure 5(a). Moreover, we notice that the peaks in the spin up and down probabilities, for large E , are shifted in energy by the exchange term value $|H_{ex}|$. For example, the spin up ($\eta = 1$) peak in the transmission probability for the AC direction with $\varepsilon = 0.1$ is situated at $E \approx 10.7 meV$ and thus the counterpart peak in the spin down ($\eta = -1$) is located at $E - H_{ex} \approx 10.1 meV$. On the other hand, applying the AC strain to the sample completely alters the transmission profile and increase the overall transmission, see Figure 5(b). This is a manifestation of the different band structure alignments along the carrier propagation direction induced by the ZZ and AC strains.

Figure 6 shows the transmission probability as a function of the width ω of the strained region for up/down spin and two values of the energy. It is clearly seen that, for a fixed value of the energy, the transmission is maximal for a very thin barrier. By increasing the width of the central region,

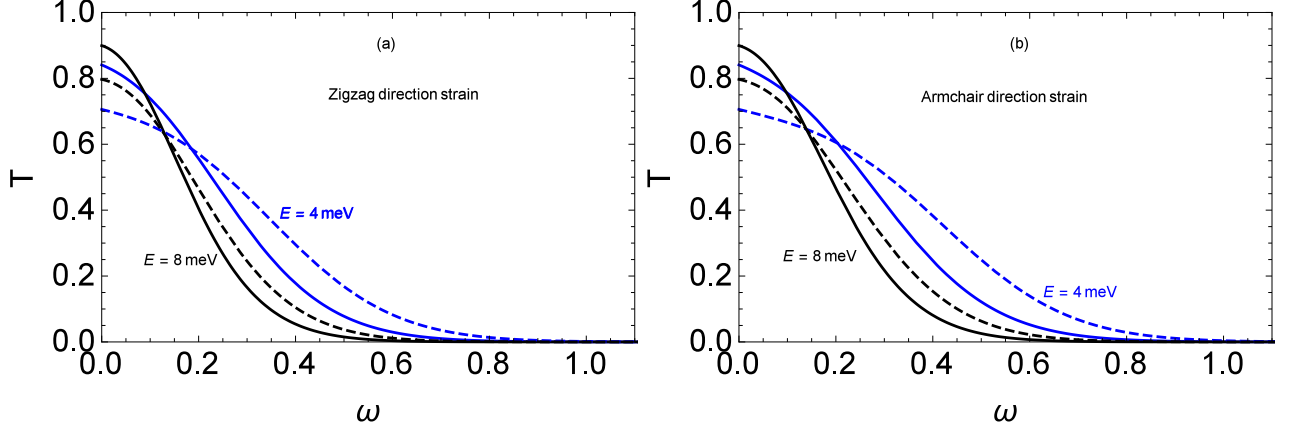


Figure 6: (color online) Transmission probability as a function of the width of the central region ω for spin up $\eta = +1$ (solid line) and spin down $\eta = -1$ (dashed line). (a)/(b): Effects of zigzag/armchair strain direction. Other parameters are $\gamma_\eta = 38.1^\circ$, $H_{ex} = 0.61$ meV, $V_b = 1.50$ meV, $V_0 = 6$ meV, $\varepsilon = 0.03$, $l_B = 0.5$ nm, $E = 4$ meV (blue line) and $E = 8$ meV (black line).

the transmission decreases until it reaches zero at a specific value of ω . It is important to note that the transmission, for the two values of the energy, are nearly the same for both AC and ZZ strains. On the other hand, the spin up transmission, for a thin barrier, is larger than the spin down one. By increasing ω , the situation will be reversed and the spin down transmission becomes larger than the spin up one for both AC and ZZ strains.

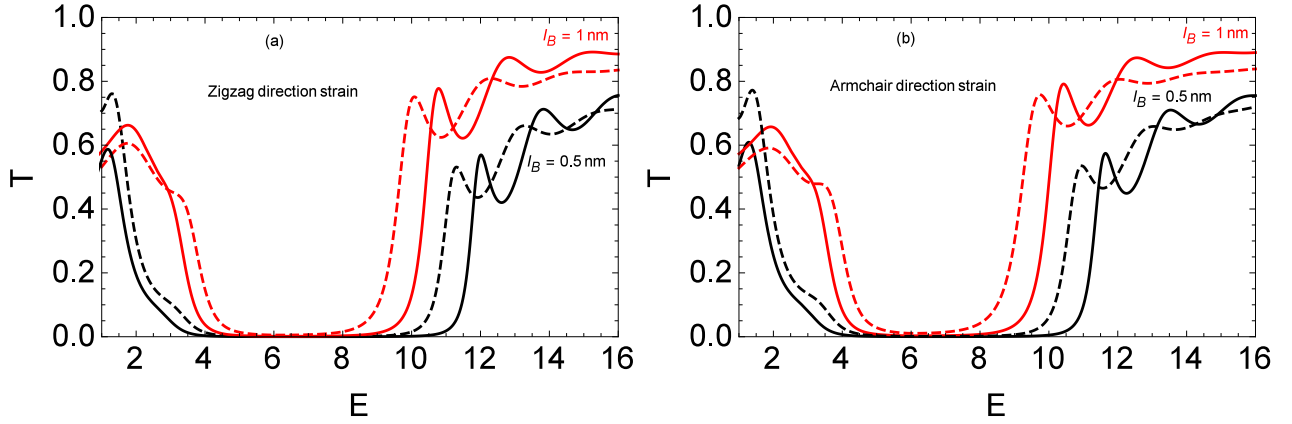


Figure 7: (color online) Transmission probability as a function of the energy with different values of the magnetic length l_B for spin up/down $\eta = +/ - 1$ (solid/dashed lines). (a)/(b): Effects of zigzag/armchair strain direction. Other parameters are $\gamma_\eta = 38^\circ$, $\omega = 0.8$ nm, $H_{ex} = 0.61$ meV, $V_b = 1.50$ meV, $V_0 = 6$ meV and $\varepsilon = 0.03$.

In Figure 7, we plot the transmission probability as a function of the energy for different values of the magnetic length. It is found that, like in Figure 5, the transmission is minimal and reaches zero at certain values of the energy, which corresponds to a forbidden zone. Moreover, one can clearly show that by increasing the magnetic field the forbidden zone becomes wider. Note that the forbidden zone will be widened if the deformation is along the AC direction. We observe that the forbidden zone

corresponding to spin up transmission is always larger than that of spin down for both ZZ and AC strains. In addition, we see clearly that some peaks are shown up and their energy positions vary with tuning the magnetic field. We notice that the transmission difference between spin up and spin down is small before the forbidden zone. However, the difference becomes more important for large values of the energy.

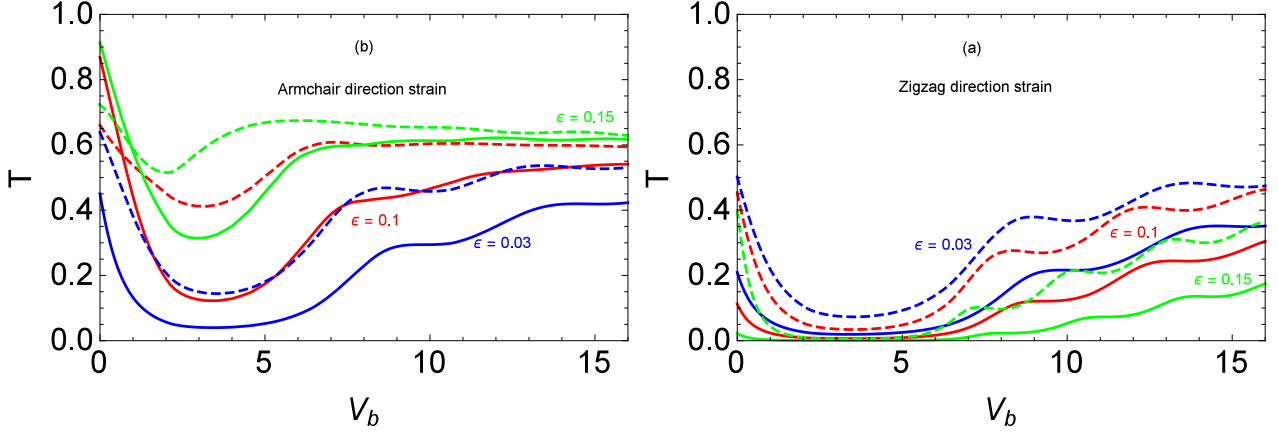


Figure 8: (color online) Transmission probability as a function of the bias V_b with different strains $\varepsilon = 0.03$ (blue line), $\varepsilon = 0.1$ (red line) and $\varepsilon = 0.15$ (green line) for spin up/down $\eta = +/ - 1$ (solid/dashed lines). (a)/(b): Effects of zigzag/armchair strain directions with $\gamma_\eta = 38^\circ$, $\omega = 0.8 \text{ nm}$, $H_{ex} = 0.61 \text{ meV}$, $E = 4 \text{ meV}$, $V_0 = 6 \text{ meV}$, $l_B = 1 \text{ nm}$.

In Figure 8, we investigate the transmission as a function of the bias V_b for different strain magnitudes. It is clearly shown that, for $V_b = 0$ we have a transmission that decreases until it reaches a minimal value by increasing the bias. For large values of the bias, the transmission starts increasing and exhibits some oscillations that are, then, relatively damped. It is important to note that the spin up and down transmission have almost the same form, but the spin down transmission is always larger. For the AC strain, we see that the transmission increases up to a specific V_b value and then reaches almost a constant value. Moreover, when the bias V_b is near zero (for the AC strain) the transmission is maximal, which is not the case for the ZZ strain.

5 Conclusion

We have investigated the transport properties of a ferromagnetic/strained/normal graphene junctions where a magnetic field is applied in the central region. After writing down the corresponding Hamiltonian, the eigenvalue equation has been solved in each region composing our system to end up with the solutions of the energy spectrum. These have been used together with the transfer matrix approach and density current to determine the transmission and reflection probabilities in terms of the physical parameters characterizing our system.

Our numerical results showed that in the first region (I) the spin up and down bands are shifted by an amount equal to the exchange energy H_{ex} and left the whole spectrum linear as in the case of pristine graphene. However, in the third region (III), it is found that the energy bands are still linear like in the case of pristine graphene, but shifted down by V_b . Moreover, by changing the values of

the applied magnetic field, the position of the Dirac point changes due to the uniaxial strain. In the strained region (II) we have showed that the application of deformation leads to a renormalization of the Fermi velocity, *i.e.* $v_F^* = \xi v_F$ and the magnetic field leaves the energy spectrum quantized, which results in the so-called Landau Levels (LLs). As a results, we have found that due to the applied strain, the LLs are contracted with respect to the pristine graphene. Our numerical results showed also that by increasing the strain magnitudes, under the same magnetic field, both the energy and distance between the LLs decrease, which is due to the fact that the applied strain affects the cyclotron orbital motion.

We have studied the transmission probabilities, for two directions of strain including zigzag (ZZ) and armchair (AC), as a function of the incident energy, width of the central region and electrostatic gate V_b . It is found that the transmission exhibits a forbidden zone ($T = 0$), at a certain values of the energy, when the strain deformation is along either the ZZ or AC directions. In addition, the width of this zone increases by increasing the strength of the strain along the ZZ direction but decreases for the AC strain. The situation was quite different by tuning the applied magnetic field because the width of the forbidden zone increases with decreasing magnetic field for either the ZZ or AC strain directions. Therefore, some peaks occur in the transmission and their energy position are changed by altering the strain magnitude. Moreover, we have observed that, for low energy, the difference between the spin up and down transmission is small before the forbidden zone and becomes more important after that. On other hand, we have found that by increasing the width of the strained region the transmission decreases and reaches zero. Moreover, the transmission increases to reach a minimal value for small values of the electrostatic gate V_b and as long as V_b is increased the transmission increased up to a specific value and reached almost constant. The spin up and down transmission have almost the same form, but the spin down transmission is almost always larger.

Acknowledgments

The generous support provided by the Saudi Center for Theoretical Physics (SCTP) is highly appreciated by all authors. AJ and HB acknowledge the support of King Fahd University of Petroleum and minerals under research group project RG171007.

References

- [1] K. S. Novoselov, A. K. Geim, S. V. Morozov, D. Jiang, Y. Zhang, S. V. Dubonos, I. V. Grigorieva and A. A. Firsov, *Science* 306, 666 (2004).
- [2] M. I. Katsnelson, K. S. Novoselov and A. K. Geim, *Nat. Phys.* 2, 620 (2005).
- [3] N. Stander, B. Huard and D. Goldhaber-Gordon, *Phys. Rev. Lett.* 102, 026807 (2009).
- [4] G. W. Semenoff, *Phys. Rev. Lett.* 53, 2449 (1984).
- [5] K. I. Bolotin, K. J. Sikes, Z. Jiang, G. Fudenberg, J. Hone, P. Kim and H. L. Stormer, *Solid State Commun.* 146, 351 (2008).

- [6] N. Tombros, C. Jozsa, M. Popinciuc, H. T. Jonkman and B. J. van Wees, *Nature* 448, 571 (2007).
- [7] H. Haugen, D. Huertas-Hernando and A. Brataas, *Phys. Rev. B* 77, 115406 (2008).
- [8] Y. Semenov, K. Kim and J. Zavada, *Appl. Phys. Lett.* 91, 153105 (2007).
- [9] A. G. Swartz, P. M. Odenthal, Y. Hao, R. S. Ruoff and R. K. Kawakami, *ACS Nano* 6, 10063 (2012).
- [10] T. Yokoyama, *Phys. Rev. B* 77, 073413 (2008).
- [11] L. Dell'Anna and A. De Martino, *Phys. Rev. B* 80, 155416 (2009).
- [12] M. Khodas, I. A. Zaliznyak and D. Kharzeev, *Phys. Rev. B* 80, 125428 (2009).
- [13] Z. Niu, *J. Appl. Phys.* 111, 103712 (2012).
- [14] Q.-P. Wu, Z.-F. Liu, A.-X. Chen, X.-B. Xiao and Z.-M. Liu, *Appl. Phys. Lett.* 105, 252402 (2014).
- [15] N. Levy, S. A. Burke, K. L. Meaker, M. Panlasigui, A. Zettl, F. Guinea, A. H. Castro Neto and M. F. Crommie, *Science* 329, 544 (2010).
- [16] V. M. Pereira, A. H. Castro Neto and N. M. R. Peres, *Phys. Rev. B* 80, 045401 (2009).
- [17] B. Soodchomshom, *Physica B* 406, 614 (2011).
- [18] Z. H. Ni, T. Yu, Y. H. Lu, Y. Y. Wang, Y. P. Feng and Z. X. Shen, *ACS Nano* 2, 2301 (2008).
- [19] T. M. G. Mohiuddin, A. Lombardo, R. R. Nair, A. Bonetti, G. Savini, R. Jalil, N. Bonini, D. M. Basko, C. Galiotis, N. Marzari, K. S. Novoselov, A. K. Geim and A. C. Ferrari, *Phys. Rev. B* 79, 205433 (2009).
- [20] M. Y. Huang, H. G. Yan, C. Y. Chen, D. H. Song, T. F. Heinz and J. Hone, *Proc. Natl. Acad. Sci. U.S.A.* 106, 7304 (2009).
- [21] A. H. Castro Neto, F. Guinea, N. M. R. Peres, K. S. Novoselov and A. K. Geim, *Rev. Mod. Phys.* 81, 109 (2009).
- [22] M. M. Fogler, F. Guinea and M. I. Katsnelson, *Phys. Rev. Lett.* 101, 226804 (2008).
- [23] V. M. Pereira and A. H. Castro Neto, *Phys. Rev. Lett.* 103, 046801 (2009).
- [24] S.-M. Choi, S.-H. Jhi and Y.-W. Son, *Phys. Rev. B* 81, 081407(R)(2010).
- [25] Y. Wang, Y. Liu and B. Wang, *Appl. Phys. Lett.* 105, 052409 (2014).
- [26] F. M. D. Pellegrino, G. G. N. Angilella and R. Pucci, *Phys. Rev. B* 84, 195404 (2011).
- [27] Y. Wang, Y. Liu and B. Wang, *Appl. Phys. Lett.* 103, 182603 (2013).
- [28] M. O. Goerbig, J.N. Fuchs, G. Montambaux and F. Piéchon, *Phys. Rev. B* 78, 045415 (2008).
- [29] Y. Betancur-Ocampo, M. E. Cifuentes-Quintal, G. Courdourier-Maruri and R. de Coss, *Ann. Phys. (N. Y.)* 359, 243 (2015).